



# Delineation of the visual pathway in paediatric optic pathway glioma patients using probabilistic tractography, and correlations with visual acuity

Patrick W. Hales<sup>a,\*</sup>, Victoria Smith<sup>b</sup>, Deepi Dhanoa-Hayre<sup>b</sup>, Patricia O'Hare<sup>c</sup>, Kshitij Mankad<sup>d</sup>, Felice d'Arco<sup>d</sup>, Jessica Cooper<sup>d</sup>, Ramneek Kaur<sup>a</sup>, Kim Phipps<sup>c</sup>, Richard Bowman<sup>b</sup>, Darren Hargrave<sup>c</sup>, Christopher Clark<sup>a</sup>

<sup>a</sup> Developmental Imaging & Biophysics Section, University College London Great Ormond Street Institute of Child Health, London, UK

<sup>b</sup> Ophthalmology Department, Great Ormond Street Children's Hospital, London, UK

<sup>c</sup> Haematology and Oncology Department, Great Ormond Street Children's Hospital, London, UK

<sup>d</sup> Radiology Department, Great Ormond Street Children's Hospital, London, UK

## ARTICLE INFO

### Keywords:

Optic pathway glioma  
Diffusion MRI  
Tractography  
Cancer  
Constrained spherical deconvolution

## ABSTRACT

**Background:** Radiological biomarkers which correlate with visual function are needed to improve the clinical management of optic pathway glioma (OPG) patients. Currently, these are not available using conventional magnetic resonance imaging (MRI) sequences. The aim of this study was to determine whether diffusion MRI could be used to delineate the entire optic pathway in OPG patients, and provide imaging biomarkers within this pathway which correlate with a patient's visual acuity (VA).

**Methods:** Multi-shell diffusion MRI data were acquired in a cohort of paediatric OPG patients, along with VA measurements in each eye. Diffusion MRI data were processed using constrained spherical deconvolution and probabilistic fibre tractography, to delineate the white matter bundles forming the optic pathway in each patient. Median fractional anisotropy (FA) and apparent diffusion coefficient (ADC) were measured in the optic nerves, tracts, and radiations, and correlated against each patient's VA.

**Results:** In the optic nerves, median FA significantly correlated with VA ( $R_{\text{adj}}^2 = 0.31$ ,  $p = 0.0082$ ), with lower FA associated with poorer vision. In the optic radiations, both lower FA and higher ADC were significantly associated with poorer vision ( $R_{\text{adj}}^2 = 0.52$ ,  $p = 0.00075$  and  $R_{\text{adj}}^2 = 0.50$ ,  $p = 0.0012$  respectively). No significant correlations between VA and either FA or ADC were found in the optic tracts.

**Conclusions:** Multi-shell diffusion MRI provides *in vivo* delineation of the optic pathway in OPG patients, despite the presence of tumour invasion. This technique provides imaging biomarkers which are sensitive to micro-structural damage to the underlying white matter in this pathway, which is not always visible on conventional MRI.

## 1. Introduction

Optic pathway glioma (OPG) is a childhood tumour of the visual pathway, which is often associated with the genetic disorder neurofibromatosis type 1 (NF1). Despite having low-grade histological features, in keeping with World Health Organisation (WHO) grade I pilocytic astrocytoma (Cummings et al., 2000), OPGs are diffusively infiltrative, and tend to course along the optic nerves, chiasm, tracts, and, less frequently, the optic radiations. As such, despite their low malignancy, approximately one-third to one-half of OPG patients suffer visual loss as a result of their tumour (Balcer et al., 2001; Listernick et al., 1994).

The lack of well-defined tumour margins, as well as the risk of

damage to the visual apparatus, mean OPGs are not easily amenable to surgical resection (Aquilina et al., 2015), and chemotherapy is generally the first line of treatment. However, determining when to treat patients remains a challenging clinical problem. A previous epidemiological study showed that no presenting factor (such as age, tumour location, and NF1-associated symptoms) could predict the need for future treatment (King et al., 2003). Furthermore, there are currently no radiological techniques which can reliably predict loss of vision in patients (Aquilina et al., 2015; Fisher et al., 2012; Shofty et al., 2011; Ahn et al., 2006). Although magnetic resonance imaging (MRI) is widely used in the management of OPG patients, tumour extent on 'conventional' MRI does not correlate with visual impairment (Fisher et al., 2012; Shofty et al., 2011; de Blank et al., 2013; Mitchell et al.,

\* Corresponding author at: Developmental Imaging & Biophysics Section, UCL Great Ormond Street Institute of Child Health, 30 Guilford Street, London WC1N 1EH, UK.  
E-mail address: [p.hales@ucl.ac.uk](mailto:p.hales@ucl.ac.uk) (P.W. Hales).

2001; Campagna et al., 2010). As such, there is a clinical need for an imaging biomarker which is sensitive to microstructural tumour invasion of the optic pathway, and correlates directly with a patient's visual function.

Diffusion MRI is a semi-quantitative imaging technique, which can be used to obtain detailed information about white matter pathways in the human brain (Basser et al., 1994). The signal in diffusion MRI is sensitised to the random diffusion of water molecules, and the regular arrangement of tightly packed bundles of axons in the brain introduces a directional dependence to this diffusion. By measuring the degree of diffusion along a number of non-collinear directions, the degree of directionality (quantified by the fractional anisotropy, FA) and the magnitude of diffusion (quantified by the apparent diffusion coefficient, ADC), can be measured. It has been suggested that these parameters can act as surrogate biomarkers of 'integrity' and 'density' of the local neuronal axons, respectively, (Beaulieu, 2002; Assaf and Pasternak, 2008) although this interpretation will be confounded by additional factors such as partial volume effects with cerebral spinal fluid (CSF), crossing fibres within an imaging voxel, cell membrane permeability, etc. (Vos et al., 2011; Wheeler-Kingshott and Cercignani, 2009; Jones et al., 2013). By following a path through local fibre orientation estimates, 'fibre tractography' can be performed to infer the long-range white matter tracts connecting distant brain regions (Mori and van Zijl, 2002).

Diffusion tensor imaging (DTI) is the most widely used model to measure white matter orientation (Basser et al., 1994), and is being increasingly used in the planning of neurosurgical investigations (Romano et al., 2009; Trivedi et al., 2008). DTI is an attractive option due to the relatively low scan-time requirements, and relative simplicity of the post-processing. However, the tensor model is known to be invalid in imaging voxels containing multiple fibre pathways that cross or pass very close to each other (Jeurissen et al., 2014; Pierpaoli et al., 2001; Alexander et al., 2001; Frank, 2001), resulting in erroneous estimates of both white matter anatomy and axonal integrity (Pierpaoli et al., 2001; Tournier et al., 2011; Behrens et al., 2007; Jones and Cercignani, 2010; Vos et al., 2012). As it has been estimated that crossing fibres occur in over 90% of white matter voxels in a typical clinical DTI study (Jeurissen et al., 2010), this can have serious implications for the accuracy of this technique.

Constrained spherical deconvolution (CSD) provides an alternative post-processing model for diffusion MRI data, in which a 'fibre orientation distribution function' (fODF) is estimated in each imaging voxel, allowing multiple fibre orientations to be resolved (Tournier et al., 2004; Tournier et al., 2007). This has led to improved reliability of tractography throughout the brain (Jeurissen et al., 2011), and specifically, CSD-based tractography has been shown to improve the delineation of the optic radiations in patients with high-grade gliomas, compared to DTI-based tractography (Mormina et al., 2016).

CSD modelling requires acquisitions with a larger number of diffusion-encoding directions (typically around 60), and has traditionally been used with 'single-shell' data, in which diffusion is measured at a single level of diffusion weighting (known as the b-value). Recently, a 'multi-shell' CSD method has been proposed, which models diffusion data acquired at multiple b-values (Jeurissen et al., 2014). This technique utilises the unique signal response to increasing b-value of different tissue types in the brain (e.g. white matter (WM), grey matter (GM), and CSF) in order to separate out the contributions from each in the diffusion signal. This technique, known as multi-shell, multi-tissue CSD (MSMT-CSD), provides an improvement over single-shell CSD, which suffers from unreliable, noisy fODF estimates in voxels containing a mixture of tissue types (Jeurissen et al., 2014; Dell'acqua et al., 2010; Roine et al., 2014).

A number of previous studies have explored the clinical benefits of diffusion MRI in OPG patients. Yeom et al. (2013) showed that OPG tumours with a higher ADC at baseline were more likely to progress and require treatment. Nickerson et al. (2010) measured reduced FA and

increased ADC in the optic nerves of patients with lesions intrinsic to the optic nerve (some of which were OPG lesions). In both these studies, measurements were acquired by manually placing regions of interest (ROIs) in either the tumour or the optic nerves. In contrast to this, however, diffusion-based fibre tractography can potentially delineate the axonal pathways that form the entire optic pathway. This would be beneficial as compromised structural integrity at any point along this pathway will affect a patient's visual acuity (VA). However, tractography of the optic pathway is technically challenging. The anatomy of the optic chiasm requires crossing fibres to be adequately resolved. Furthermore, the proximity of the optic nerves and chiasm to regions of magnetic field inhomogeneities, caused by the differential magnetic susceptibility of air and tissue, lead to marked distortions in the echo-planar imaging (EPI) readout typically used in diffusion MRI.

A recent study by de Blank et al. (2013) used DTI-based fibre tractography to delineate the optic pathway in a cohort of paediatric OPG patients, and found reduced FA in the optic radiations was associated with VA loss. However, no significant correlations were found in the optic nerves or tracts, which may be due to limitations of the diffusion tensor model described above.

In this study, we investigated whether more advanced diffusion imaging, based on the MSMT-CSD model, could provide a delineation of the entire optic pathway in patients suffering from OPG. Having identified this pathway, we hypothesised that diffusion-MRI-derived measures of axonal structure in the optic nerves, tracts, and optic radiations would correlate with VA, which would demonstrate the potential of this technique to detect microstructural damage to the visual pathway, which may not be visible on conventional MRI.

## 2. Methods

Twenty-six patients being treated or monitored for OPG at our institution were included in this study. All patients were receiving regular ophthalmological and MRI assessment on a 3–6 monthly basis as part of their care, and MRI examinations were matched to the closest ophthalmological assessment for each patient. Approval for this study was granted by our institutional ethical review board. Patients or patient's guardians (depending on patient age) provided written informed consent. In three patients, diffusion MRI had been included as part of their clinical care, for whom retrospective access to imaging data was granted.

### 2.1. Ophthalmology evaluation

All patients were assessed at the ophthalmology clinic at our institution, by a paediatric ophthalmologist. Visual acuity was measured using an age-appropriate testing method (Teller, logMAR Kays, or logMAR), after which all visual scores were converted to the equivalent logarithm of the minimum angle of resolution (logMAR) score (Sloan, 1959), to allow comparison across patients. On the logMAR scale, a value of 0 represents '20/20' vision, and increasing logMAR scores represent poorer vision (for example, '20/200' vision has a logMAR score of 1.0) (Sloan, 1959). Vision was measured independently in each eye, where possible.

### 2.2. Magnetic resonance imaging

All imaging was performed on a Siemens 3.0 T Prisma scanner (Siemens, Erlangen, Germany), equipped with a 20 channel head receive coil. Multi-shell diffusion MRI was performed in conjunction with the standard clinical MRI protocols in use at our institution, which included an axial T2-weighted (T2w) turbo spin-echo acquisition, fluid attenuated inversion recovery (FLAIR) sequences, and pre- and post-gadolinium T1w acquisitions.

The multi-shell diffusion sequence employed a diffusion-weighted spin-echo single shot 2D EPI acquisition, with multi-banded radio

frequency pulses to accelerate volume coverage along the slice direction (Setsompop et al., 2012a; Setsompop et al., 2012b). We employed a multi-band factor of 2 over 66 slices of 2 mm thickness with 0.2 mm slice gap. Diffusion gradients were applied over two ‘shells’:  $b = 1000 \text{ s/mm}^2$  and  $b = 2200 \text{ s/mm}^2$ , with 60 non-co-linear diffusion directions per shell, in addition to 13 interleaved  $b_0$  (non-diffusion weighted) images. Other imaging parameters were: TR = 3050 ms, TE = 60 ms, field of view =  $220 \times 220 \text{ mm}$ , matrix size =  $110 \times 110$ , in-plane voxel resolution = 2.0 mm, GRAPPA factor 2, phase-encoding (PE) partial Fourier = 6/8. An additional  $b_0$  acquisition was performed, with identical readout to the diffusion-weighted scan, but with the PE direction flipped by  $180^\circ$  (in the anterior-posterior direction), for correction of susceptibility-related artefacts (see Post-processing). The total scan time for the multi-shell diffusion sequence (including the  $b_0$  acquisition with flipped PE) was 7 min 50 s.

### 2.3. Post-processing

By combining the diffusion-weighted data with the PE-flipped  $b_0$  image, the susceptibility-induced off-resonance field was estimated and corrected using a method similar to (Andersson et al., 2003), as implemented in *FSL* (fMRIB, Oxford University). Further eddy-current-induced distortions were corrected using *FSL*. All subsequent image post-processing was performed using the *MRtrix 3.0* software package (Brain Research Institute, Melbourne, Australia).

Full details of the MSMT-CSD processing technique, and subsequent tractography, are given in *Supplementary Materials, S1*. In brief, after estimation of voxel-wise WM fODFs, a probabilistic streamlines algorithm was used to delineate the optic nerves, optic tracts, and optic radiations in each patient. This was performed in a piecewise manner, allowing these individual components of the optic pathway to be identified, on the left/right sides of the brain. An example of the final tracts in a representative patient is illustrated in Fig. 1. Following identification of these tracts, median values of FA and ADC were measured in each region (see *Supplementary Materials, S1.1*).

### 2.4. Tumour identification

Tumour ROIs were manually drawn by a paediatric neuro-radiologist, using *FSL* software (fMRIB, Oxford, UK). Tumours were defined as regions of hyper-intensity and/or abnormal increase in size on the T2w  $b_0$  image, using the T2w, FLAIR and T1w post-contrast clinical images for guidance. In order to compare the tumour locations across the cohort, a group-wise registration was performed to bring all tumour ROIs into a common space (see *Supplementary Materials, S-1.2*).

### 2.5. Statistical analysis

Statistical analysis was performed using Matlab (version R2016b, MathWorks Inc., Natick, MA). A significance level of 5% was used in all statistical tests, and Benjamini & Hochberg False Discovery Rate (FDR) correction (Benjamini and Hochberg, 1995) was used to correct for multiple comparisons, where applicable. Linear regression was used to investigate the relationship between measured values of VA and imaging parameters. In the linear regression models, VA (measured using the logMAR score) was used as the response variable. The predictor variable of interest was either median FA or median ADC (separate models were used for each), measured in the optic nerves, tracts, or radiations. Patient age, NF1 status and active treatment status (i.e. whether the patient was receiving chemotherapy at the time of imaging) were included as additional predictor variables. Initially, linear regression models were fit using all predictor variables. Backward stepwise regression was then used to determine a final model, in which the least significant terms were progressively removed. After removing each term, an F-test was used to compare the goodness of fit of the reduced/nested model

compared to the full model. This process was repeated until the combination of predictors was found which minimised the  $p$ -value associated with the F-test. After determining the final linear regression models, a ‘leave-one-out’ analysis was performed to measure prediction accuracy. For this, each patient in turn was excluded from the pool of raw data, and the linear regression model (based on the significant predictors determined above) was fit to the remaining patients. Using this, the difference between the predicted and measured logMAR score for the excluded patient was recorded. After repeating this over all the patients, the root mean square of the prediction error of the final model was recorded.

For the optic nerves, VA in the eye with the highest measureable logMAR score (i.e. the worst measureable eye) was correlated directly against the imaging parameters in the corresponding optic nerve (e.g. if VA was worst in the left eye, this was correlated against median FA or ADC in the left optic nerve). However, the same technique could not be used for the optic tracts and radiations, as, being posterior to the optic chiasm, these receive input from both eyes. Here, mean inter-eye VA was used as the response variable. Median FA or ADC across both optic tracts was the first predictor variable, median FA or ADC across both optic radiations was the second predictor variable, and patient age, NF1 status and active treatment status were included as additional predictors.

Patients for which VA in one eye was too poor to be quantified using a logMAR score were excluded from the linear regression analysis. An additional group-wise analysis was performed in order to include these patients. Group 1 was defined as all patients having VA of  $\leq 0.5$  logMAR (the WHO defines VA  $> 0.5$  logMAR as part of the criteria for low-vision). Group 2 included all patients with VA  $> 0.5$  logMAR, or with un-measurable VA in one eye. Similar to the linear regression modelling, for the optic nerves, we matched VA in the worst eye to the imaging parameters in the corresponding optic nerve. For the optic tracts and radiations, VA was averaged across both eyes, and imaging parameters were averaged across the left and right optic tracts and radiations.

## 3. Results

### 3.1. Patient characteristics

The median interval between visual assessment and MRI was 18 days (range 1 to 189 days), and median patient age was 6.2 years (range 1.4 to 16.9 years). Fourteen of the patients were NF1 positive (NF1+) and 12 were NF1 negative (NF1−). Seven patients were on active treatment with chemotherapy at the time of imaging (median 75 days of treatment), and one of these patients had also received previous enucleation of the right eye and removal of the right optic nerve.

Six of the patients in our cohort had VA in their worst eye which was too poor to be quantified (2 of which were NF1+). Of these, 4 had no perception of light, and 2 could detect hand-movements only. Of the 20 patients with measureable VA in both eyes, the mean logMAR score in the best eye was  $0.43 (\pm 0.52, \text{standard deviation})$ , and  $0.73 (\pm 0.73)$  in the worst eye ( $p = 1.0$ , Wilcoxon signed rank test). Of these, there was no significant difference between VA in the NF1+ group (median worst-eye logMAR =  $0.64 \pm 0.86$ ,  $N = 12$ ), and the NF1− group (worst-eye logMAR =  $0.87 \pm 0.48$ ,  $N = 8$ ;  $p = 0.11$ , two-sided Wilcoxon rank sum test).

The NF1+ patients in our cohort had significantly lower median ADC in the optic nerves than the NF1− patients ( $8.37 \times 10^{-4} \text{ mm}^2/\text{s}$  cf.  $9.27 \times 10^{-4} \text{ mm}^2/\text{s}$  respectively,  $p = 0.028$ , two-tailed  $t$ -test). In the optic tracts, the NF1+ patients had significantly higher median FA than the NF1− patients ( $0.37$  cf.  $0.33$ ,  $p = 0.035$ , two-tailed  $t$ -test). No other significant differences between NF1+ and NF1− patients were found in the optic pathway.

A map of ‘tumour incidence’ is shown in Fig. 2. Overall, 46% of

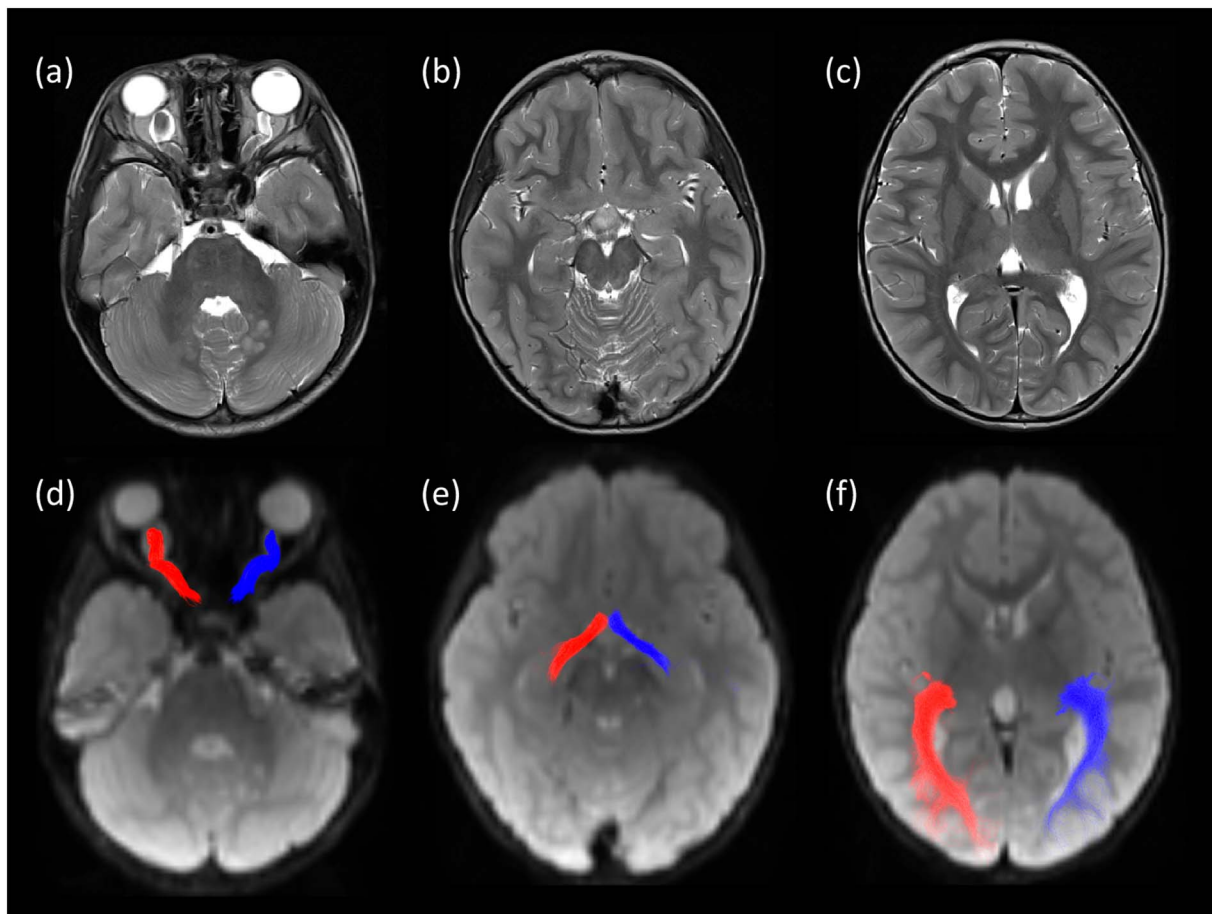


**Fig. 1.** Axial T2w clinical images (a–c), and corresponding slices from the  $b_0$  image from the diffusion scan (d–f), in a representative patient. The streamlines from probabilistic fibre tractography are overlaid, delineating the optic nerves (d), optic tracts (e), and optic radiations (f). Right- and left-hand sides are shown in red and blue respectively. (For interpretation of the references to colour in this figure legend, the reader is referred to the web version of this article.)

patients showed radiological evidence (on conventional MRI) of tumour involvement in the optic nerves, 42% showed tumour involvement of the optic tracts, and 15% showed tumour involvement of the optic radiations.

### 3.2. Linear regression analysis

In the optic nerve FA model, backward stepwise regression eliminated NF1 status, age and active treatment as non-significant predictors of worst-eye VA. The final model included only median FA in the optic nerve, which was a significant predictor of VA in corresponding eye ( $R^2_{\text{adj}} = 0.31$ , FDR-corrected  $p = 0.0082$ ), with lower FA associated with poorer vision. The root-mean-square (RMS) prediction error from the leave-one-out analysis was 0.65 logMAR units for this model. In the optic nerve ADC model, no significant predictors remained after backward stepwise regression.

In the optic tracts and radiations, the only significant predictor of mean inter-eye VA in the final FA model was median FA in the optic radiations ( $R^2_{\text{adj}} = 0.52$ , FDR-corrected  $p = 0.00075$ , RMS prediction error = 0.44 logMAR units), with lower optic radiation FA associated with poorer vision. Median FA in the optic tracts was not a significant predictor of mean inter-eye VA. Similarly, in the ADC model, median ADC in the optic radiations was a significant predictor of mean inter-eye VA (FDR-corrected  $p = 0.0012$ ), with higher ADC in the optic radiations being associated with poorer vision, but the same was not true in the optic tracts. In the ADC model, NF1 status was also a significant predictor of mean inter-eye VA (FDR-corrected  $p = 0.045$ ), with NF1 – being associated with poorer vision ( $R^2_{\text{adj}} = 0.50$  for combined ADC/

NF1 model,  $p = 0.0012$ , RMS prediction error = 0.44 logMAR units). Individual plots of VA vs. median FA, and VA vs. median ADC, along the optic pathway, are shown in Fig. 3.

### 3.3. Group-wise analysis

Box plots of FA and ADC values in the optic nerves, tracts, and radiations for the two groups are shown in Fig. 4. There was no significant difference in median FA in the optic nerves in Group 1 ( $VA \leq 0.5$ ) compared to Group 2 ( $VA > 0.5$  or un-measurable; Group 1 = 0.34, Group 2 = 0.28, FDR-corrected  $p = 0.1287$ , two-tailed  $t$ -test). Similarly, there was no significant difference in optic nerve median ADC between the two groups (Group 1 =  $8.3 \times 10^{-4} \text{ mm}^2/\text{s}$ , Group 2 =  $8.7 \times 10^{-4} \text{ mm}^2/\text{s}$ , FDR-corrected  $p = 0.36$ ). In the optic tracts, no significant difference was found between the two groups in either median FA (Group 1 = 0.38, Group 2 = 0.33, FDR-corrected  $p = 0.16$ ) or median ADC (Group 1 =  $8.3 \times 10^{-4} \text{ mm}^2/\text{s}$ , Group 2 =  $8.7 \times 10^{-4} \text{ mm}^2/\text{s}$ , FDR-corrected  $p = 0.61$ ). In the optic radiations, median FA was significantly higher in Group 1 (FA = 0.55) compared to Group 2 (FA = 0.50, FDR-corrected  $p = 0.026$ ). There was no significant difference median ADC in optic radiations between the two groups (Group 1 =  $6.9 \times 10^{-4} \text{ mm}^2/\text{s}$ , Group 2 =  $7.2 \times 10^{-4} \text{ mm}^2/\text{s}$ , FDR-corrected  $p = 0.16$ ).

## 4. Discussion

In this study, we demonstrated the feasibility of acquiring high angular resolution multi-shell diffusion data in a clinical setting, with



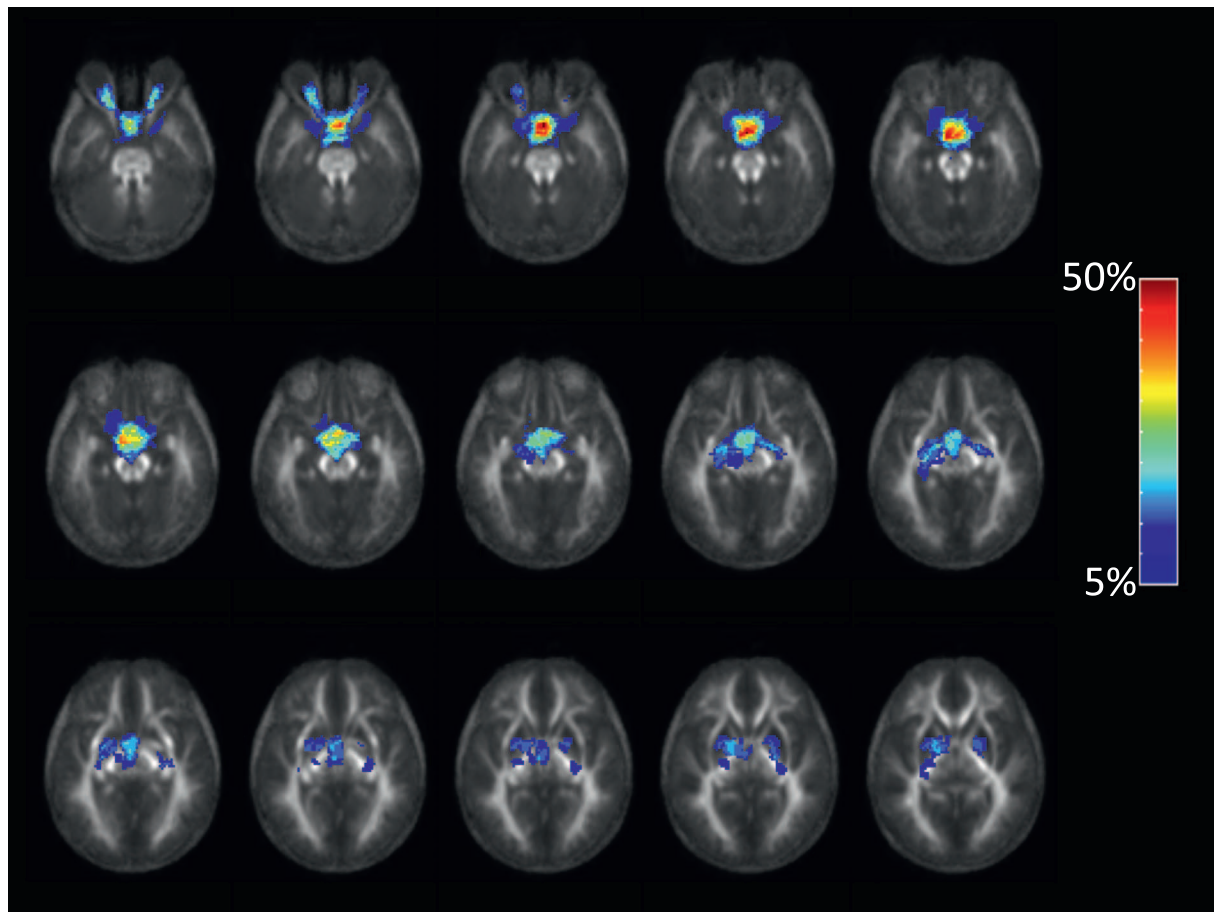


**Fig. 2.** Tumour incidence map. The background greyscale images show axial slices from the mean FA map, after affine co-registration of all patient's FA maps into a common space. The colour overlay represents the percentage of patients with evidence of tumour in a given voxel, as defined by hyper-intensity on T2w imaging. (For interpretation of the references to colour in this figure legend, the reader is referred to the web version of this article.)

sufficient diffusion-encoding to perform MSMT-CSD. Using this technique, we were able to perform probabilistic tractography to delineate the entire optic pathway in paediatric OPG patients, despite the challenges of crossing fibres in the chiasm and tumour invasion of the pathway. The acquisition of phase-encoding-reversed  $b_0$  images facilitated the delineation of the optic nerves, which has previously proved challenging due to susceptibility-induced off-resonance field artefacts in this region (de Blank et al., 2013).

In the optic nerves and optic radiations, decreased FA values were strongly associated with poorer vision. In the optic radiations, increased ADC was also strongly associated with poorer vision. A similar pattern was seen for the optic radiation FA measurements in the group analysis, with higher FA in Group 1, which represents patients with near-normal vision, compared to Group 2, representing patients with poor vision or un-measurable vision in one eye.

Similar to the findings in our study, a reduction in optic nerve FA was previously reported in children with intrinsic optic nerve pathology (including OPG) in (Nickerson et al., 2010), although this was not measured against VA, and the optic nerves were defined manually, rather than using tractography. A negative correlation between VA and FA was reported in the optic radiations in a paediatric cohort of NF1 + OPG patients (de Blank et al., 2013), but in this study no correlations between VA and FA/ADC were found in the optic nerves.

Similar to tumour-invasion of other white matter pathways in the brain, changes in FA and ADC in the optic pathway may represent microstructural damage caused by dislocation or infiltration of white matter bundles, or vasogenic oedema (Mormina et al., 2016; Witwer et al., 2002). In addition, anterograde degeneration from disruption to

visual input may lead to 'downstream' structural alterations along the optic pathway (de Blank et al., 2013; Lober et al., 2012; Beatty et al., 1982). Although these cannot easily be disentangled, our study suggests that multi-shell diffusion MRI provides improved sensitivity to the underlying structure of the white matter bundles forming the visual pathway, which may be undetectable on conventional MRI. For instance, on T2w imaging, the tumours in our cohort were mostly concentrated in the chiasm, with the majority of the optic radiations appearing unaffected (Fig. 2). However, the relationship between FA/ADC and vision was by far the strongest in the optic radiations, despite a lack of obvious tumour involvement in this region in most patients. In addition to the microstructural effects described above, this could be due, in part, to the larger size of the optic radiations, making their accurate delineation using tractography more feasible. Both the optic tracts and optic nerves are smaller in size, and as such, erroneous inclusion or exclusion of tissue in these regions will have greater impact on the relationship with VA. Susceptibility-induced distortions are also significant in the region of the optic tracts, which may not have been fully corrected using the phase-encoding reversed  $b_0$  images. Furthermore, although the optic nerves and optic tracts are similar in size, imaging parameters in the optic nerves were compared directly to vision in the corresponding eye. This one-to-one relationship could not be used for the optic tracts, which both receive input from both eyes. This, combined with their small size, may explain the lack of correlation between FA/ADC in the optic tracts and VA.

In this study, patient age and active treatment status were not found to be significant predictors of VA. Although normal vision varies with age in younger children (Leone et al., 2014; Sonksen et al., 2008), our

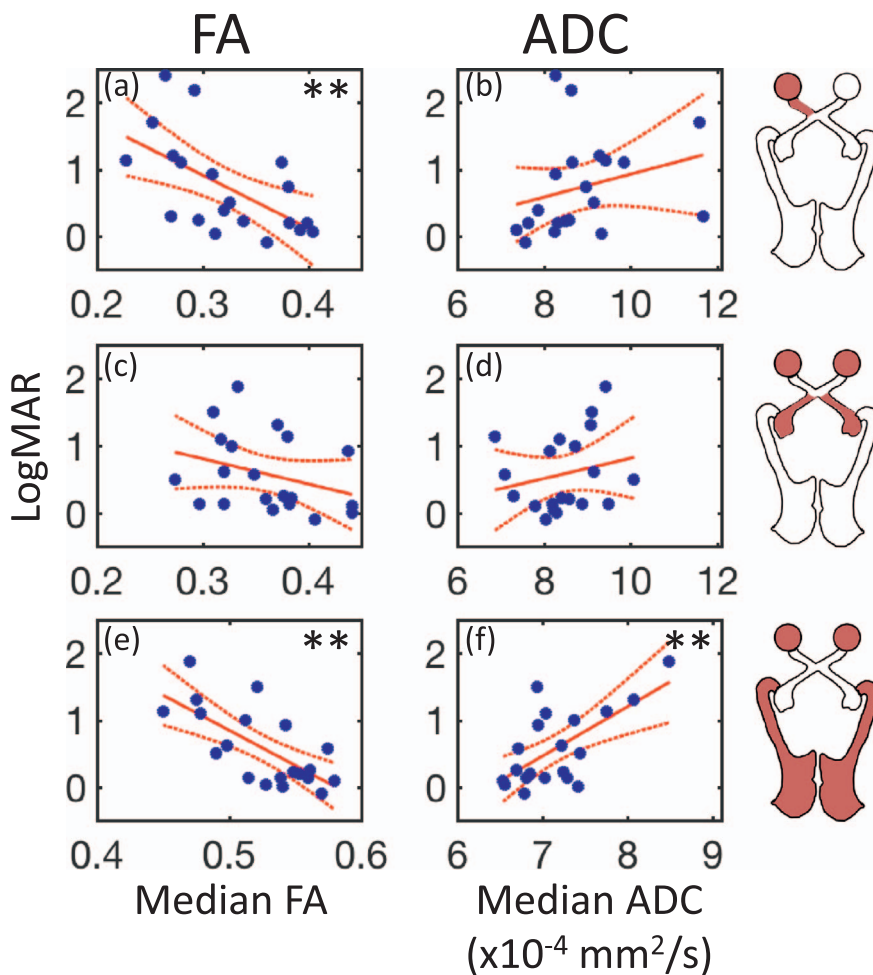


**Fig. 3.** Individual correlations between VA (in logMAR units) vs. median FA (left column), and VA vs. median ADC (right column). Data for worst-eye VA vs. FA/ADC values in the corresponding optic nerve are shown on the top row (a,b). Data for mean inter-eye VA vs. mean FA/ADC values for the optic tracts are shown on the middle row (c,d), and mean inter-eye VA vs. mean FA/ADC values for the optic radiations on the bottom row (e,f). Data points for individual patients are shown as blue circles, with the linear fit shown as a red solid line, and the 95% confidence interval of the fit shown in red dashed lines (\*\* $p < 0.01$  for linear regression model, after FDR-correction for multiple comparisons). (For interpretation of the references to colour in this figure legend, the reader is referred to the web version of this article.)

data suggest that, in the presence of tumour invasion of the optic pathway, the structural properties of the optic nerves and radiations far outweigh any age-related or treatment-related effects on vision.

When comparing the structural properties of the optic pathway in the NF1 + and NF1 – group (ignoring VA), we observed lower ADC in the NF1 + patients in the optic nerves, and increased FA in the NF1 + patients in the optic tracts. This could be indicative of reduced white matter integrity in the NF1 – patients in these regions, compared to NF1 + patients. However, when the combined influence of both NF1 status and FA/ADC on VA was considered, NF1 status generally had no significant effect on vision. The one exception to this was in the optic tract/radiation ADC model, in which NF1 status had a small influence on VA, with NF1 + patients having better vision. However, the influence of median ADC in the optic radiations on VA in the same model was an order of magnitude more significant. Overall, this suggests that the structural properties of the optic nerves and radiations, represented by FA/ADC, have by far the greatest influence on VA, but there may be a weak effect of NF1 status, with NF1 + patients having slightly better vision. The latter would support the data presented in (Jost et al., 2008), in which OPGs in NF1 – patients were shown to be more clinically aggressive (defined as causing significant visual decline) than OPGs in NF1 + patients.

This study had a number of limitations. Firstly, visual field assessments were not available for the patients included in this study. This prevented us from directly correlating deficits in vision in the left/right hemifield against the structural properties of the corresponding optic tract or radiation, which may have led to improved correlations between imaging and VA. Furthermore, techniques such as visual evoked potential recordings, which are thought to represent the integrity of the

afferent visual pathway, may well show improved correlation with FA/ADC measurements in the optic pathway. In the absence of visual field data, imaging parameters in the optic tracts and radiations were correlated against mean inter-eye visual acuity in this study. Although this metric is not generally used clinically (a patient's visual function is more strongly linked to their best eye visual acuity), this was considered to be the most biologically relevant metric when assessing the structural integrity of the visual pathway in regions which receive input from both eyes.

In addition, FA and ADC values were used as predictors of visual acuity in this study. Although the correlation between these parameters in the optic radiations and a patient's visual acuity was highly significant, the large root-mean-square prediction errors of these models suggest that these metrics alone would not be suitable for accurately predicting a patient's vision. The size of these prediction errors was influenced in part by the inclusion of patients with severely impaired vision in our correlation analysis, which, combined with the young age of these patients, make an accurate assessment of visual acuity extremely challenging. In addition, further factors, such as retinal thickness, will affect a patient's vision, which were not included in this study.

Furthermore, although FA and ADC are widely used when demonstrating tumour infiltration of white matter pathways, these parameters have some well-known limitations in terms of acting as a surrogate biomarker of nerve fibre integrity/density (Vos et al., 2011; Wheeler-Kingshott and Cercignani, 2009). For instance, within a given imaging voxel, partial volume with CSF, axonal diameter, cell membrane permeability, and the degree of axonal myelination can all influence these parameters, and disentangling these using diffusion-MRI data alone is extremely challenging (Jones et al., 2013).

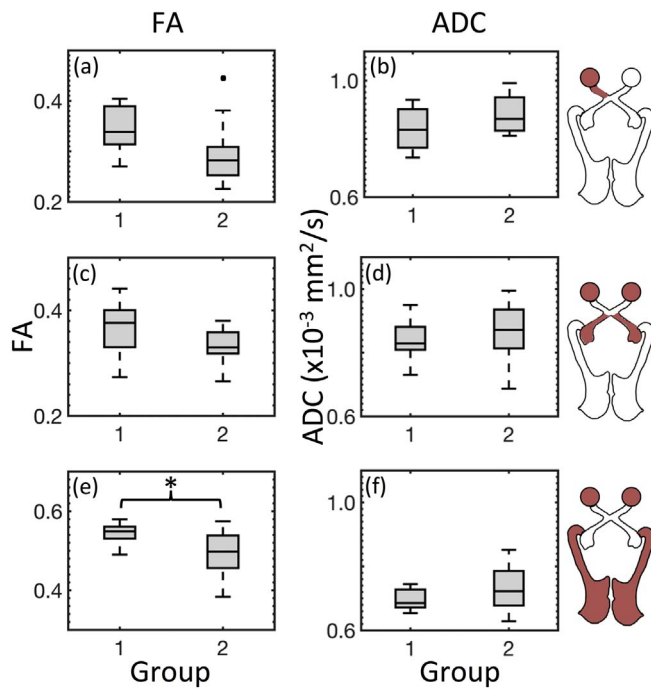


**Fig. 4.** Box plots from the group-wise analysis. Group 1 included patients with VA  $\leq 0.5$ , Group 2 included patients with VA  $> 0.5$ , or un-measurable VA in one eye. Median FA values are shown on the left column, median ADC values are shown on the right. Data for worst-eye VA vs. FA/ADC values in the corresponding optic nerve are shown on the top row (a,b). Data for mean inter-eye VA vs. mean FA/ADC values for the optic tracts are shown on the middle row (c,d), and mean inter-eye VA vs. mean FA/ADC values for the optic radiations on the bottom row (e,f). (\* $p < 0.05$  after FDR-correction for multiple comparisons).

Finally, the data presented here represent a cross-sectional study, in which the relationship between FA/ADC in the optic pathway and vision was explored. A longitudinal study using the same imaging techniques would allow the predictive power of early changes in FA/ADC on a patient's vision to be explored. Previous studies have shown preliminary data to suggest that baseline values of diffusion metrics in the optic radiations (de Blank et al., 2013), or in the tumour itself (Yeom et al., 2013), may be predictive of subsequent changes in VA, and the tractography techniques presented here may present an optimal methodology for exploring this further.

## 5. Conclusion

Multi-shell, multi-tissue CSD can be performed in a clinically feasible scan time, and provides sufficient information to delineate the entire optic pathway in paediatric OPG patients. This allows the optic pathway to be identified on FA or ADC maps, which in turn allows the structural properties of the white matter forming the optic pathway to be measured. In the optic nerves and optic radiations, these metrics have a significant correlation with a patient's vision. This relationship was strongest in the optic radiations - a region in which the majority of our patients showed no sign of tumour involvement on conventional clinical imaging. As such, diffusion MRI may provide *in vivo* identification of damage to the optic pathway which would not be visible otherwise. As FA in the optic radiations provides the most sensitive correlate of VA, this measure could potentially be explored as a prognostic indicator of future decline of visual function.

## Acknowledgments

The authors would like to thank the patients who have participated in this study, and the staff at Great Ormond Street Hospital for

assistance in acquiring the data. We also thank the University of Minnesota Center for Magnetic Resonance Research for providing the multiband-EPI sequence (<http://www.cmrr.umn.edu/multiband>). This work was supported by Great Ormond Street Children's Charity and Children with Cancer UK (CwCuk-15-203).

## Appendix A. Supplementary data

Supplementary data to this article can be found online at <https://doi.org/10.1016/j.nicl.2017.10.010>.

## References

- Ahn, Y., Cho, B.-K., Kim, S.-K., et al., 2006. Optic pathway glioma: outcome and prognostic factors in a surgical series. *Childs Nerv. Syst.* 22 (9), 1136–1142. <http://dx.doi.org/10.1007/s00381-006-0086-7>.
- Alexander, A.L., Hasan, K.M., Lazar, M., Tsuruda, J.S., Parker, D.L., 2001. Analysis of partial volume effects in diffusion-tensor MRI. *Magn. Reson. Med.* 45 (5), 770–780.
- Andersson, J.L.R., Skare, S., Ashburner, J., 2003. How to correct susceptibility distortions in spin-echo echo-planar images: application to diffusion tensor imaging. *NeuroImage* 20 (2), 870–888. [http://dx.doi.org/10.1016/S1053-8119\(03\)00336-7](http://dx.doi.org/10.1016/S1053-8119(03)00336-7).
- Aquilina, K., Daniels, D.J., Spoudeas, H., Phipps, K., Gan, H.-W., Boop, F.A., 2015. Optic pathway glioma in children: does visual deficit correlate with radiology in focal exophytic lesions? *Childs Nerv. Syst.* 31 (11), 2041–2049. <http://dx.doi.org/10.1007/s00381-015-2855-7>.
- Assaf, Y., Pasternak, O., 2008. Diffusion tensor imaging (DTI)-based white matter mapping in brain research: a review. *J. Mol. Neurosci.* 34 (1), 51–61. <http://dx.doi.org/10.1007/s12031-007-0029-0>.
- Balcer, L.J., Liu, G.T., Heller, G., et al., 2001. Visual loss in children with neurofibromatosis type 1 and optic pathway gliomas: relation to tumor location by magnetic resonance imaging. *Am. J. Ophthalmol.* 131 (4), 442–445.
- Basser, P.J., Mattiello, J., LeBihan, D., 1994. Estimation of the effective self-diffusion tensor from the NMR spin echo. *J. Magn. Reson. B* 103, 247–254.
- Beatty, R., Sadun, A., Smith, L., Vonsattel, J., Richardson, E., 1982. Direct demonstration of transsynaptic degeneration in the human visual system: a comparison of retrograde and anterograde changes. *J. Neurol. Neurosurg. Psychiatry* 45 (2), 143–146.
- Beaulieu, C., 2002. The basis of anisotropic water diffusion in the nervous system - a technical review. *NMR Biomed.* 15 (7–8), 435–455. <http://dx.doi.org/10.1002/nbm.782>.
- Behrens, T.E.J., Berg, H.J., Jbabdi, S., Rushworth, M.F.S., Woolrich, M.W., 2007. Probabilistic diffusion tractography with multiple fibre orientations: what can we gain? *NeuroImage* 34 (1), 144–155. <http://dx.doi.org/10.1016/j.neuroimage.2006.09.018>.
- Benjamini, Y., Hochberg, Y., 1995. Controlling the false discovery rate: a practical and powerful approach to multiple testing. *J. R. Stat. Soc. Ser. B Methodol.* 57 (1), 289–300.
- de Blank, P.M.K., Berman, J.I., Liu, G.T., Roberts, T.P.L., Fisher, M.J., 2013. Fractional anisotropy of the optic radiations is associated with visual acuity loss in optic pathway gliomas of neurofibromatosis type 1. *Neuro-Oncology* 15 (8), 1088–1095. <http://dx.doi.org/10.1093/neuonc/not068>.
- Campagna, M., Opocher, E., Viscardi, E., et al., 2010. Optic pathway glioma: long-term visual outcome in children without neurofibromatosis type-1. *Pediatr. Blood Cancer* 55 (6), 1083–1088. <http://dx.doi.org/10.1002/pbc.22748>.
- Cummings, T.J., Provenzale, J.M., Hunter, S.B., et al., 2000. Gliomas of the optic nerve: histological, immunohistochemical (MIB-1 and p53), and MRI analysis. *Acta Neuropathol.* 99 (5), 563–570.
- Dell'acqua, F., Scifo, P., Rizzo, G., et al., 2010. A modified damped Richardson-Lucy algorithm to reduce isotropic background effects in spherical deconvolution. *NeuroImage* 49 (2), 1446–1458. <http://dx.doi.org/10.1016/j.neuroimage.2009.09.033>.
- Fisher, M.J., Loguidice, M., Gutmann, D.H., et al., 2012. Visual outcomes in children with neurofibromatosis type 1-associated optic pathway glioma following chemotherapy: a multicenter retrospective analysis. *Neuro-Oncology* 14 (6), 790–797. <http://dx.doi.org/10.1093/neuonc/nos076>.
- Frank, L.R., 2001. Anisotropy in high angular resolution diffusion-weighted MRI. *Magn. Reson. Med.* 45 (6), 935–939.
- Jeurissen, B., Leemans, A., Tournier, J.-D., Jones, D.K., Sijbers, J., 2010. In: *Estimating the number of fiber orientations in diffusion MRI Voxels: a constrained spherical deconvolution study*. Proceedings of the International Society for Magnetic Reso. Stockholm, Sweden. pp. 573.
- Jeurissen, B., Leemans, A., Jones, D.K., Tournier, J.-D., Sijbers, J., 2011. Probabilistic fiber tracking using the residual bootstrap with constrained spherical deconvolution. *Hum. Brain Mapp.* 32 (3), 461–479. <http://dx.doi.org/10.1002/hbm.21032>.
- Jeurissen, B., Tournier, J.-D., Dhollander, T., Connelly, A., Sijbers, J., 2014. Multi-tissue constrained spherical deconvolution for improved analysis of multi-shell diffusion MRI data. *NeuroImage* 103, 411–426. <http://dx.doi.org/10.1016/j.neuroimage.2014.07.061>.
- Jones, D.K., Cercignani, M., 2010. Twenty-five pitfalls in the analysis of diffusion MRI data. *NMR Biomed.* 23 (7), 803–820. <http://dx.doi.org/10.1002/nbm.1543>.
- Jones, D.K., Knösche, T.R., Turner, R., 2013. White matter integrity, fiber count, and other fallacies: the do's and don'ts of diffusion MRI. *NeuroImage* 73 (Supplement C), 239–254. <http://dx.doi.org/10.1016/j.neuroimage.2012.06.081>.

- Jost, S.C., Ackerman, J.W., Garbow, J.R., Manwaring, L.P., Gutmann, D.H., McKinstry, R.C., 2008. Diffusion-weighted and dynamic contrast-enhanced imaging as markers of clinical behavior in children with optic pathway glioma. *Pediatr. Radiol.* 38 (12), 1293–1299. <http://dx.doi.org/10.1007/s00247-008-1003-x>.
- King, A., Listernick, R., Charrow, J., Piersall, L., Gutmann, D.H., 2003. Optic pathway gliomas in neurofibromatosis type 1: the effect of presenting symptoms on outcome. *Am. J. Med. Genet. A* 122A (2), 95–99. <http://dx.doi.org/10.1002/ajmg.a.20211>.
- Leone, J.F., Mitchell, P., Kifley, A., Rose, K.A., 2014. Sydney Childhood Eye Studies. Normative visual acuity in infants and preschool-aged children in Sydney. *Acta Ophthalmol.* 92 (7), e521–529. <http://dx.doi.org/10.1111/aos.12366>.
- Listernick, R., Charrow, J., Greenwald, M., Mets, M., 1994. Natural history of optic pathway tumors in children with neurofibromatosis type 1: a longitudinal study. *J. Pediatr.* 125 (1), 63–66. [http://dx.doi.org/10.1016/S0022-3476\(94\)70122-9](http://dx.doi.org/10.1016/S0022-3476(94)70122-9).
- Lober, R.M., Guzman, R., Cheshier, S.H., Fredrick, D.R., Edwards, M.S.B., Yeom, K.W., 2012. Application of diffusion tensor tractography in pediatric optic pathway glioma. *J. Neurosurg. Pediatr.* 10 (4), 273–280. <http://dx.doi.org/10.3171/2012.7.PEDS1270>.
- Mitchell, A.E.M.B.C.B., Elder, J.E.M.B.B.S., Mackey, D.A.M.D., Waters, K.D.M.B.B.S., Ashley, D.M., 2001. Visual improvement despite radiologically stable disease after treatment with carboplatin in children with progressive low-grade optic/thalamic gliomas. *J. Pediatr. Hematol. Oncol.* 23 (9), 572–577.
- Mori, S., van Zijl, P.C.M., 2002. Fiber tracking: principles and strategies - a technical review. *NMR Biomed.* 15 (7–8), 468–480. <http://dx.doi.org/10.1002/nbm.781>.
- Mormina, E., Arrigo, A., Calamuneri, A., et al., 2016. Optic radiations evaluation in patients affected by high-grade gliomas: a side-by-side constrained spherical deconvolution and diffusion tensor imaging study. *Neuroradiology* 58 (11), 1067–1075. <http://dx.doi.org/10.1007/s00234-016-1732-8>.
- Nickerson, J.P., Salmela, M.B., Koski, C.J., Andrews, T., Filippi, C.G., 2010. Diffusion tensor imaging of the pediatric optic nerve: intrinsic and extrinsic pathology compared to normal controls. *J. Magn. Reson. Imaging* 32 (1), 76–81. <http://dx.doi.org/10.1002/jmri.22228>.
- Pierpaoli, C., Barnett, A., Pajevic, S., et al., 2001. Water diffusion changes in Wallerian degeneration and their dependence on white matter architecture. *NeuroImage* 13 (6 Pt 1), 1174–1185. <http://dx.doi.org/10.1006/nimg.2001.0765>.
- Roine, T., Jeurissen, B., Perrone, D., et al., 2014. Isotropic non-white matter partial volume effects in constrained spherical deconvolution. *Front. Neuroinform.* 8, 28. <http://dx.doi.org/10.3389/fninf.2014.00028>.
- Romano, A., D'Andrea, G., Minniti, G., et al., 2009. Pre-surgical planning and MR-tractography utility in brain tumour resection. *Eur. Radiol.* 19 (12), 2798–2808. <http://dx.doi.org/10.1007/s00330-009-1483-6>.
- Setsompop, K., Cohen-Adad, J., Gagoski, B.A., et al., 2012a. Improving diffusion MRI using simultaneous multi-slice echo planar imaging. *NeuroImage* 63 (1), 569–580. <http://dx.doi.org/10.1016/j.neuroimage.2012.06.033>.
- Setsompop, K., Gagoski, B.A., Polimeni, J.R., Witzel, T., Wedeen, V.J., Wald, L.L., 2012b. Blipped-controlled aliasing in parallel imaging for simultaneous multislice echo planar imaging with reduced g-factor penalty. *Magn. Reson. Med.* 67 (5), 1210–1224. <http://dx.doi.org/10.1002/mrm.23097>.
- Shofty, B., Ben-Sira, L., Freedman, S., et al., 2011. Visual outcome following chemotherapy for progressive optic pathway gliomas. *Pediatr. Blood Cancer* 57 (3), 481–485. <http://dx.doi.org/10.1002/pbc.22967>.
- Sloan, L.L., 1959. New test charts for the measurement of visual acuity at far and near distances. *Am. J. Ophthalmol.* 48, 807–813.
- Sonksen, P.M., Wade, A.M., Proffitt, R., Heavens, S., Salt, A.T., 2008. The Sonksen logMAR test of visual acuity: II. Age norms from 2 years 9 months to 8 years. *J. AAPOS* 12 (1), 18–22. <http://dx.doi.org/10.1016/j.jaapos.2007.04.019>.
- Tournier, J.-D., Calamante, F., Gadian, D.G., Connelly, A., 2004. Direct estimation of the fiber orientation density function from diffusion-weighted MRI data using spherical deconvolution. *NeuroImage* 23 (3), 1176–1185. <http://dx.doi.org/10.1016/j.neuroimage.2004.07.037>.
- Tournier, J.-D., Calamante, F., Connelly, A., 2007. Robust determination of the fibre orientation distribution in diffusion MRI: non-negativity constrained super-resolved spherical deconvolution. *NeuroImage* 35 (4), 1459–1472. <http://dx.doi.org/10.1016/j.neuroimage.2007.02.016>.
- Tournier, J.-D., Mori, S., Leemans, A., 2011. Diffusion tensor imaging and beyond. *Magn. Reson. Med.* 65 (6), 1532–1556. <http://dx.doi.org/10.1002/mrm.22924>.
- Trivedi, R., Rathore, R.K., Gupta, R.K., 2008. Review: clinical application of diffusion tensor imaging. *Indian J. Radiol. Imaging* 18 (1), 45–52. <http://dx.doi.org/10.4103/0971-3026.38505>.
- Vos, S.B., Jones, D.K., Viergever, M.A., Leemans, A., 2011. Partial volume effect as a hidden covariate in DTI analyses. *NeuroImage* 55 (4), 1566–1576. <http://dx.doi.org/10.1016/j.neuroimage.2011.01.048>.
- Vos, S.B., Jones, D.K., Jeurissen, B., Viergever, M.A., Leemans, A., 2012. The influence of complex white matter architecture on the mean diffusivity in diffusion tensor MRI of the human brain. *NeuroImage* 59 (3), 2208–2216. <http://dx.doi.org/10.1016/j.neuroimage.2011.09.086>.
- Wheeler-Kingshott, C.A.M., Cercignani, M., 2009. About “axial” and “radial” diffusivities. *Magn. Reson. Med.* 61 (5), 1255–1260. <http://dx.doi.org/10.1002/mrm.21965>.
- Witwer, B.P., Moftakhar, R., Hasan, K.M., et al., 2002. Diffusion-tensor imaging of white matter tracts in patients with cerebral neoplasm. *J. Neurosurg.* 97 (3), 568–575. <http://dx.doi.org/10.3171/jns.2002.97.3.0568>.
- Yeom, K.W., Lober, R.M., Andre, J.B., et al., 2013. Prognostic role for diffusion-weighted imaging of pediatric optic pathway glioma. *J. Neuro-Oncol.* 113 (3), 479–483. <http://dx.doi.org/10.1007/s11060-013-1140-4>.